Nano Research

ISSN 1998-0124 CN 11-5974/O4
https://doi.org/10.1007/s12274-023-5659-1

Research Article

Low-temperature optothermal nanotweezers

Jianxing Zhou[1], Xiaoqi Dai[1], Yuhang Peng[1], Yili Zhong[1], Ho-Pui Ho[2], Yonghong Shao[1], Bruce Zhi Gao[3], Junle Qu[1], and Jiajie Chen[1] (✉)

[1] *State Key Laboratory of Radio Frequency Heterogeneous Integration; Key Laboratory of Optoelectronic Devices and Systems of Ministry of Education and Guangdong Province, College of Physics and Optoelectronics Engineering, Shenzhen University, Shenzhen 518060, China*
[2] *Department of Biomedical Engineering, The Chinese University of Hong Kong, Hong Kong 999077, China*
[3] *Department of Bioengineering and COMSET, Clemson University, Clemson, SC 29634, USA*

Received: 25 January 2023 / **Revised:** 28 February 2023 / **Accepted:** 9 March 2023

ABSTRACT

Optical tweezers that rely on laser irradiation to capture and manipulate nanoparticles have provided powerful tools for biological and biochemistry studies. However, the existence of optical diffraction-limit and the thermal damage caused by high laser power hinder the wider application of optical tweezers in the biological field. For the past decade, the emergence of optothermal tweezers has solved the above problems to a certain extent, while the auxiliary agents used in optothermal tweezers still limit their biocompatibility. Here, we report a kind of nanotweezers based on the sign transformation of the thermophoresis coefficient of colloidal particles in low-temperature environment. Using a self-made microfluidic refrigerator to reduce the ambient temperature to around 0 °C in the microfluidic cell, we can control a single nanoparticle at lower laser power without adding additional agent solute in the solution. This novel optical tweezering scheme has provided a new path for the manipulation of inorganic nanoparticles as well as biological particles.

KEYWORDS

optothermal tweezers, optical manipulation, microfluidic device, thermophoresis, thermo-osmotic flow

1 Introduction

Since the invention of optical tweezers by Ashkin [1], it has been widely used in biological [2, 3] and colloidal manipulations [4, 5]. However, the existence of diffraction limit hinders the development of optical tweezers for single nanoparticle manipulation [6]. In order to obtain a stable optical trap, higher laser power is usually required, which inevitably induces optothermal effect or even damage [7, 8]. Fortunately, plasmonic nanotweezers that based on the hot-spots excited at the nanostructure have achieved the trapping of nanoparticles at the nanostructure with low laser power [9–13], thus, reducing the thermal damage. However, the nanostructure fixed on the substrate limits the long-range manipulation of nanoparticles.

Since 2013, the invention of optothermal tweezers has enabled us to manipulate particles and cells in long-range with lower optothermal damage than traditional optical tweezers [14–22]. They normally used thermophoresis which is a generalized force that can drive suspended particles, micelles, or droplets moving along the temperature gradient field [23]. In the optothermal induced temperature field, the key point for building optothermal tweezers is to obtain a suitable thermophoresis coefficient, namely, Soret coefficient, which determines the particles migrating direction and velocity magnitude. In 2017, novel optothermal nanotweezers are developed [19, 21, 22, 24], just by adding some surfactants such as sodium dodecyl sulfate (SDS) or cetyltrimethylammonium chloride (CTAC) to modify the nanoparticle surface and building an internal thermoelectric field, they have achieved the trapping of gold nanoparticles under lower laser intensity. Lately in 2021, opto-refrigeration tweezers are developed via an optical induced cold source [25, 26], the cold source was generated by an upconversion anti-Stokes fluorescence emission of ytterbium-doped yttrium lithium fluoride (Yb:YLF) crystals [27, 28].

Therefore, the optical thermal tweezers nowadays usually rely on the auxiliary agents such as surfactants or upconversion semiconductor materials which in direct contact with target particles to facilitate an effective trap towards the heating center. However, these schemes have intrinsically brought two major issues. Firstly, the temperature increment above room temperature (25 °C) of the optothermal tweezers may still induce some side effects to trapped particles. Secondly, the auxiliary agents, such as normal cation or anion surfactants, are normally not biocompatible. These two issues have greatly hindered the development of optothermal tweezers.

To tackle the issues, herein, by tailing the expansion coefficient and hydration entropy of the solution [23, 29], so as to obtain a negative Soret coefficient of the trapped particle, we have developed low-temperature optothermal nanotweezers (LONT) microfluidic platform without adding any additional auxiliary agent. In the LONT scheme, the synergy effect of thermophoresis and thermo-osmotic flows generated around the laser heating center traps the nanoparticles. With the operation temperature range of 0–4 °C, the trapping and manipulating of polystyrene particles and gold nanoparticles are achieved. The operation laser power of LONT is in the range of 0.03–0.23 mW, corresponding

Address correspondence to cjj@szu.edu.cn

to a minimum optical power intensity of 42.5 μW/μm². In comparison, a classic optical tweezer used a 2 mW 1064 nm laser, resulting in a trapping stiffness (TS) of approximately 20 fN/μm for a single 100 nm gold particle [30]. However, LONT is capable of trapping 160 nm gold particles with a similar trapping stiffness while the laser power intensity is 1–2 orders of magnitude lower. The low operating temperature and power intensity have made this strategy a great candidate for handling biological samples. We believe that with further development, the LONT scheme can be potentially used in more applications in the field of nanotechnology and biochemistry.

2 Results and discussion

In general, the thermophoresis velocity u of particles can be described by $u = -D_T \nabla T$ [31], where D_T is the thermal diffusion coefficient. In the case of steady state, the thermal diffusion of particles in the solvent is balanced by the ordinary diffusion. The concentration of particles in the microfluidic cell is expressed as $c = c_0 \exp(-S_T T)$ ($S_T = D_T/D$, S_T is the same sign as D_T) [32], which depends on the temperature difference between the laser focused region and the ambient region and its own Soret coefficient S_T. Soret coefficient is susceptible to quite a lot of ambient parameters such as pH value, ambient temperature, particle surface charge, and size [23, 33]. A positive S_T means that the particles will be driven towards the cooler region, while a negative one means that the particles will be attracted to the hotter region, i.e., thermophilic. Generally, colloidal nanoparticles have a positive S_T [14, 25], i.e., they are normally thermophobic. Therefore, the traditional optothermal tweezers usually use additional surfactants, such as CTAC and SDS, to modify the surface of the target nanoparticles towards a thermophilic behavior [19, 22, 24], i.e., forming a negative S_T, which would drive the particle towards the hotter center. Others also used an up-conversion material via optical refrigeration to build temperature field with a cooler center [25, 26]. Therefore, nanoparticles with positive S_T can be trapped at the laser focusing center.

To build an optothermal tweezering scheme with better biocompatibility that is free from these auxiliary agents, we started to find other ways to turn the targeted nanoparticle thermophilic. Fortunately, we noticed that a decreasing ambient temperature of the flow cell can reverse the sign of S_T or D_T, so that particles can be trapped at the heat source center via laser irradiation. Furthermore, for uncharged or weakly charged particles, the non-uniform solvent caused by the temperature gradient field will make the particles obtain the following thermal diffusion coefficient [23]

$$D_T = \frac{2\beta H}{9\pi\eta d_0} \quad (1)$$

where β is the expansion coefficient of solvent, H is the Hamaker coefficient [34], η is the viscosity of solvent, and d_0 is the cut-off parameter. It can be seen from Eq. (1) that the positive and negative sign of S_T depend on the expansion coefficient (β) of solvent.

In general, a solvent is expanded upon heated, therefore, particles normally experience a positive S_T that keeps them away from the hotter side. However, water below 4 °C has a negative expansion coefficient β, which means that at this low-temperature environment condition, the D_T will become negative and it can drive the nanoparticles towards the laser heating center.

Based on the above analysis, we designed a microfluidic device composed of an optical tweezering system and a microfluidic refrigerator above the microfluidic cell shown in Figs. 1(a) and 1(b). By filling the ice-water mixture into the refrigerant chamber on the top of the microfluidic chamber together with a copper

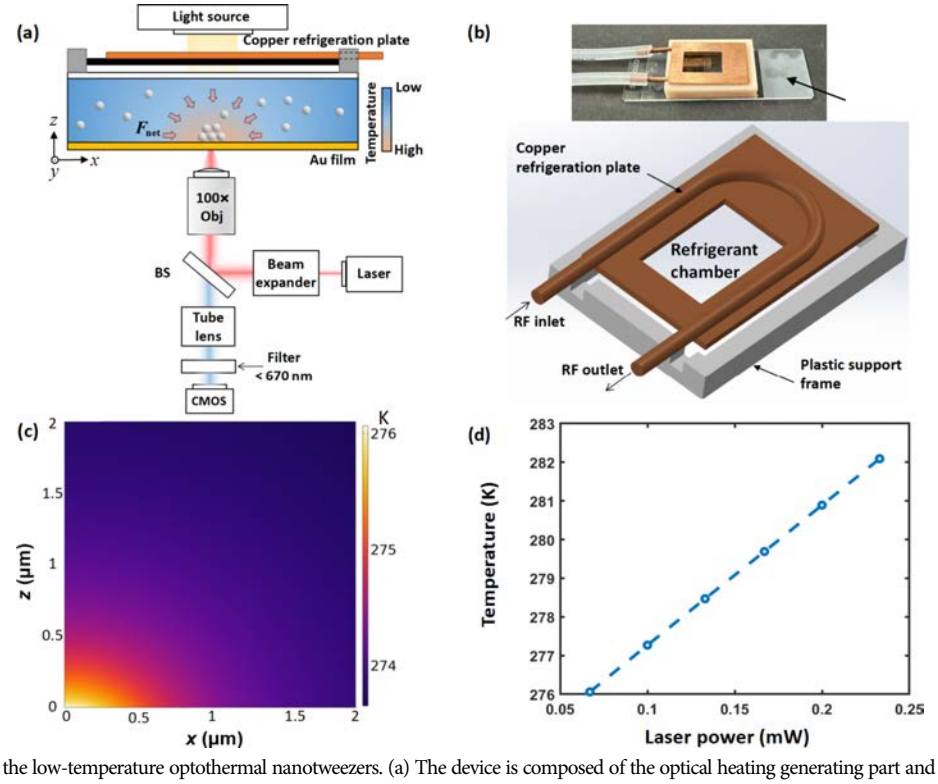

Figure 1 Schematic of the low-temperature optothermal nanotweezers. (a) The device is composed of the optical heating generating part and the refrigerant chamber above the microfluidic cell. The 785 nm laser is expanded and reflected by short wavelength pass BS before focusing at the Au film. And a bright-field microscopy and CMOS device are used for the observation. (b) The refrigerant chamber above the microfluidic cell consists of a copper refrigeration plate and a plastic support frame. The copper refrigeration plate is connected with a low-temperature controller and a peristaltic pump is adopted for the cycling of the RF inside the copper refrigeration plate, and they are attached on the top of a glass slide (76 mm × 26 mm). (c) The simulated in-plane temperature distributions around the laser center (0.0) at the laser power of 0.067 mW. (d) Maximum temperature around the laser center versus the incident laser power.

made refrigeration plate with refrigerant fluid (RF) circling inside, the ambient solution temperature in the microfluidic cell is kept at around 0 °C (see Fig. 1(c)). Therefore, we can obtain a negative D_T for the target particles. The microfluidic cell is composed of a glass slide on the top and a gold film coated cover glass seals up by thin parafilm at bottom. The thickness of the gold film is 10 nm and the height of the microfluidic cell is 30 μm. The laser irradiation on the gold film produces heating source and together with the low ambient temperature maintained by the refrigerant chamber, one can achieve the target particles manipulation inside the microfluidic chamber.

Moreover, in order to evaluate the contribution of this reversed expansion coefficient of water induced negative D_T in the manipulation, we simulated the thermophoresis force of 500 nm polystyrene (PS) particles near the heat source via finite element simulation. At laser power of 0.067 mW, where $H = 6.3 \times 10^{-20}$ J [23], $d_0 = 0.2$ nm, and ambient temperature $T_0 = 0.5$ °C (the setting of simulation is shown in Note S1 in the Electronic Supplementary Material (ESM)).

In addition, the thermo-osmotic flows on the substrate will also contribute to the trapping of particles. It is corresponding to the temperature gradient induced excess specific enthalpy at the solid–liquid interface, which leads to a flow parallel to the surface along the boundary layer [35]. The flow velocity of thermo-osmotic flow can be described as [36]

$$v = \chi \frac{\nabla T}{T} \tag{2}$$

where χ is the thermal permeability coefficient, which contains all information about the interface interaction between liquid and solid. When χ, the flow direction is in the same direction as the temperature gradient ∇T parallel to the substrate. The thermal permeation flow at the solid–liquid interface of the substrate will drive the particle flow near the substrate, and the contribution of the thermo-osmotic coefficient χ can be divided into the following two parts [21]

$$\chi_E = \frac{\varepsilon \xi^2}{8\eta} \tag{3}$$

$$\chi_{vdW} = \frac{A_H \beta T}{3\pi\eta d_0} \tag{4}$$

where $\varepsilon = 80\varepsilon_0$ is the dielectric constant of water; $\zeta = -30$ mV is the zeta potential of the substrate; $A_H = 1 \times 10^{-20}$ J is the Hamker coefficient for the PS/water/Au system; and $d_0 = 0.2$ nm is the cut-off parameter [21]. The setting of simulation of thermo-osmotic flow is shown in Note S3 in the ESM. The simulation results are shown in Fig. 2, the thermophoretic together with the thermo-osmotic flows on the substrate boundary compose the net force (F_{net}), they can drive the nanoparticles in a range of ± 2 μm travelling towards the laser heating spot center. We also calculated the corresponding trapping potential wells in terms of K_BT (shown in Fig. 2(e)), in which K_B is the Boltzmann constant. As expected, the potential well changes from a "V" to a "W" shape as laser power increases. This is because when the temperature of the trapping center exceeds 4 °C at higher laser powers, it can lead to a positive S_T. Consequently, it will generate an outward pushing force on the particles near the center region where the temperature surpasses 4 °C. In addition, the optothermal-induced nature convective flow can be ignored here, because of the shallow height of the microfluidic chamber [26, 37]. And the optical force is also negligible due to the loosely focused laser and low operational power.

Moreover, as shown in Fig. 3, we used the 500 nm PS particles (Bangs Laboratories, Inc.) in the water to demonstrate the manipulation ability of LONT. At room temperature of 25 °C, after we switched on the laser, PS particles cannot be trapped. When we started the operation of the microfluidic refrigerator and filled the refrigerant chamber with ice-water mixture, as shown in Fig. 1(c), the ambient temperature in the microfluidic cell is gradually decreased to ~ 0 °C in about 30 s. And as Fig. 3(a) shows, two PS particles are captured at the laser focusing center. When we stopped the operation of the microfluidic refrigerator and removed the ice-water mixture, the ambient temperature in

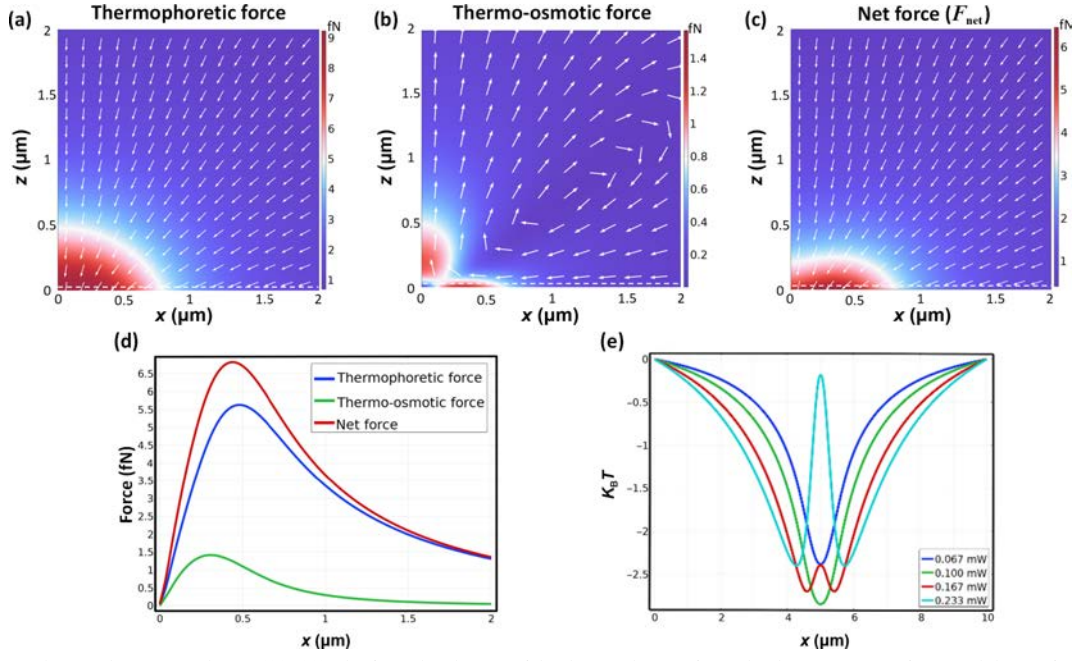

Figure 2 Force analysis in the LONT scheme. ((a)–(c)) The force distribution of the thermophoretic force, the thermo-osmotic force, and the net force (F_{net}) exerted on the 500 nm PS particles near the spot center, respectively. (d) The distribution of various forces in horizontal direction (x-axis) along the white dotted line (z = 10 nm) in ((a)–(c)), the positive value means pointing towards the laser spot center (0, 0), the laser power is 0.067 mW and the beam radius is 500 nm. (e) The trapping potential well represented by K_BT obtained in different laser powers. The force calculation detail and temperature gradient profile is shown in Notes S1–S3 in the ESM.

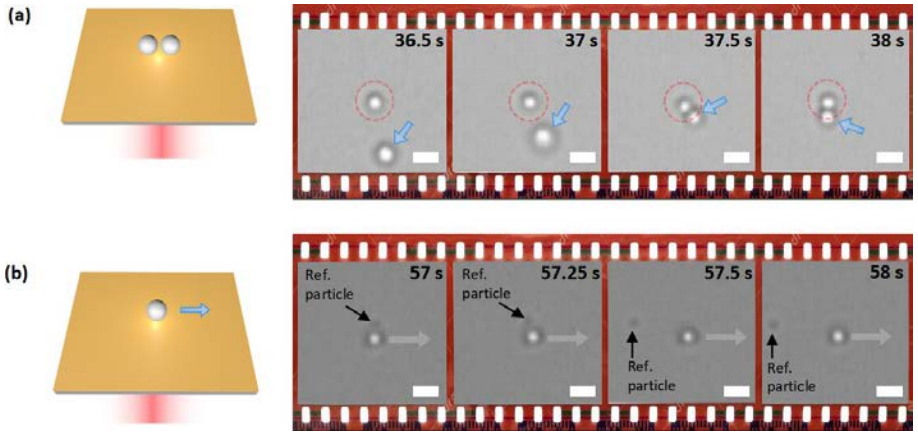

Figure 3 Nanoparticles trapping and manipulation in LONT scheme. (a) Image frames of two 500 nm-PS particles being trapped to the center of the laser spot. The laser spot is indicated by red dotted circle, and the blue arrow shows the position of PS particles moving into the trap, the laser power is 0.1 mW. The corresponding movie is shown in Movie ESM1. (b) The translation manipulation of single 500 nm-PS particle near a reference (Ref.) particle, the laser power is 0.167 mW. The scale bar is 1 μm. The room temperature is 25 °C.

the microfluidic cell started to rise, and the trapped PS particles will be pushed away and re-dispersed into the solution via Brownian motion. Thus, the trapping is indeed caused by the sign inversion of the Soret coefficient S_T of particles in the low temperature environment. And as Fig. 3(b) shows, the LONT can also achieve the translation manipulation of a single PS particle.

In order to further evaluate the trapping stability of LONT, we measured the TS by tracking the position of the trapped 500 nm PS particles via a motion blur correction method (the trapping stiffness measurement method is shown in Note S4 in the ESM) [38]. As shown in Figs. 4(c)–4(e), the trapping stiffnesses under different laser powers are presented. And we also measured the minimum laser power for supporting an effective trapping is at 0.03 mW. In addition, as Fig. 1(d) indicates, higher laser power will induce a higher temperature. While it is worth noticing that the trapping stiffness does not always increase with a higher laser power. When the laser power exceeds 0.23 mW, the PS particles will be pushed out of the trap and circled around in the thermo-osmotic flow. This is because a higher temperature (> 5 °C) in a certain area near the laser center will reverse the negative Soret coefficient to a positive one, in which the thermophoresis would push the particles away from the hotter center.

Moreover, as one can infer from the net force illustrated in Fig. 2, under 0.067 mW laser power, by taking the abnormal expansion of water and thermo-osmotic flows on the substrate boundary into account, the trapping stiffness in the horizontal direction is about 26 fN/μm. Contrary to our expectations, this theoretical one is less than the measured trapping stiffness, which is in the order of 100 fN/μm (see Fig. 4(e)). It means that in the actual PS nanoparticle trapping experiment, apart from water abnormal expansion and thermo-osmotic flow contributions, there are other factors that contribute to enhancing the negative Soret coefficient.

Therefore, we measured the zeta potential of the trapped 500 nm PS particle via the electrophoretic light scattering method (Malvern Panalytical Ltd., Zetasizer Pro), which is about −20 mV. And it has already experimentally proved that water polarization along the temperature gradient can help to trap the negative charged PS particles with a larger surface zeta potential around −50 mV at room temperature (25 °C), while a positive one cannot be trapped [39]. Therefore, here the lesser surface charge of −20 mV cannot support an effective at room temperature, only if the temperature is decreased to about 0 °C, the water abnormal expansion induced negative Soret coefficient component can further enhance a stable trap towards the hotter center.

To further verify our speculation, under the same cooling conditions, we also conducted a trapping experiment of 160 nm gold nanosphere (AuNS) (160 nm-AuNS, purchased from Nanoseedz, Inc.). And the zeta potential of 160 nm AuNS is positive (52 mV), which means there will be opposite the water polarization contributions that tend to push nanoparticles away from the hotter center. Interestingly, as shown in Fig. 4, we have also achieved the trapping and manipulation of 160 nm-AuNS (see Figs. 4(a) and 4(b)) in the LONT scheme, while the AuNS cannot be trapped at normal room temperature. Therefore, the fact that a positive charged particle can only be trapped at low-temperature condition indicates that the water abnormal expansion contributes to the trapping event. As expected, the results in Figs. 4(c)–4(e) have shown that the trapping stiffness of AuNS is quite small (10–100 fN/μm), which is in the same order of magnitude compared with our simulations. The maximum laser power to support a stable trapping of AuNS is 0.1 mW, and a higher laser power will push the AuNS away from the trap.

Nevertheless, there still exists other possible factors that contribute to the negative Soret coefficent in our LONT scheme. At a lower temperature gradient, the particle concentration $c = c_0\exp(-S_T T)$ can also be described as $c = c_0\exp[-G(T) - G(T_0)/k_B T]$ [32], where G is the Gibbs-free enthalpy of the single particle-solvent system, and T_0 is the ambient temperature. The particle Soret coefficient can also be described as [29]

$$S_T = \frac{\partial G/\partial T}{k_B T} \tag{5}$$

$$dG = -SdT + Vdp + \mu dN \tag{6}$$

after combining the above two equations, the S_T can be expressed by the entropy S: $S_T = -s/k_B T$, and S consists of two parts: the entropy of ionic shielding and the hydration entropy. The entropy of hydration will increase linearly with the decrease of temperature [40, 41], so that the sign of S_T for the particles such as proteins, DNA, and PS particles will reverse when the ambient temperature drops to a certain degree (generally 5–25 °C) [42, 43]. In fact, Duhr and coworkers have confirmed that the sign reversal of Soret coefficient occurs in both DNA and PS particles [29]. This hydration entropy correlated negative Soret coefficient may be another factor that assisted the trapping of nanoparticles in our LONT scheme.

3 Conclusions

In summary, we have developed a LONT by incorporating a self-

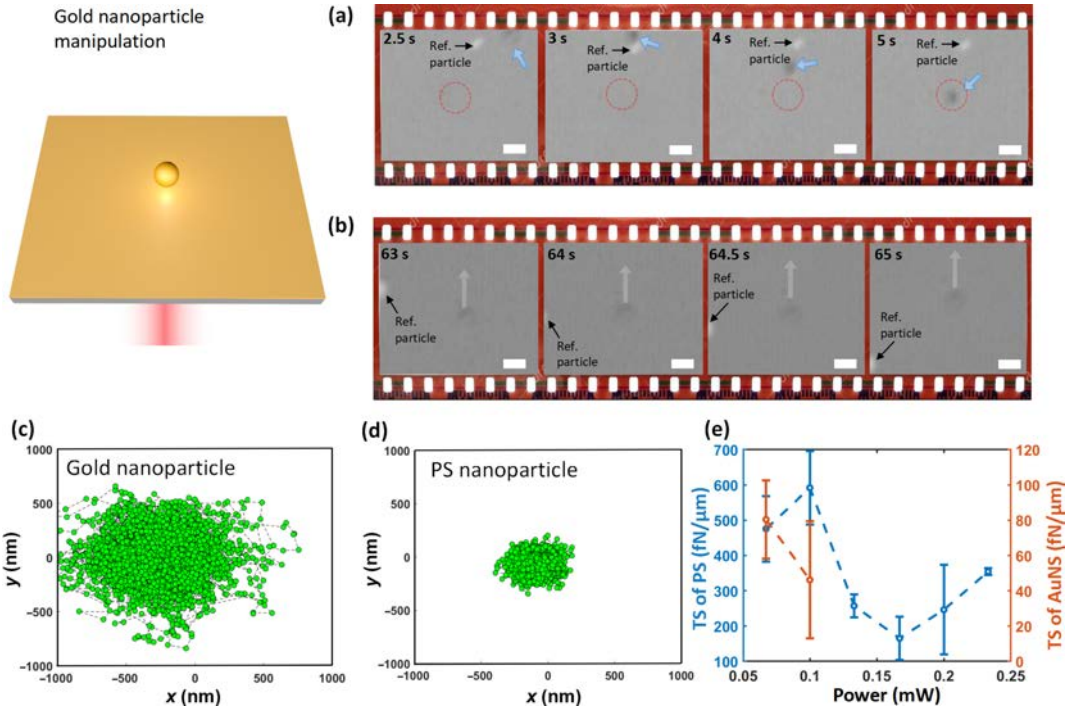

Figure 4 Gold nanoparticle trapping and trapping stiffness analysis in LONT scheme. (a) Frames of AuNS-160 nm particles being trapped towards the center of the spot. The laser spot is indicated by red dotted circle, and the blue arrow shows the position of a AuNS particle moving into the trap. (b) The translation manipulation of a single AuNS-160 nm particle near a reference particle. The laser power is 0.067 mW and the scale bar is 1 μm. ((c) and (d)) The position distribution diagram of 160 nm AuNS particle and PS nanoparticle trapping near the center of the spot under the 0.1 mW laser power. (e) The measured particle TS of the PS nanoparticle and the AuNS under different laser powers. The room temperature is 25 °C.

made microfluidic refrigerator. And our results indicate that the abnormal expansion of low-temperature water and hydration entropy have contributed to thermophoresis and thermo-osmotic force in our trapping scheme. Without adding any additional auxiliary surfactant in the solvent, LONT can reverse the Soret coefficient sign of the target particles by simply decreasing the microfluidic cell temperature, so that nanoparticles such as gold nanoparticles and polystyrene nanoparticles can be trapped. Therefore, LONT has avoided the possible auxiliary agents induced biochemical side effect on the trapped particles. In addition, the operational temperature range of LONT is 0–5 °C, which also further enhances its biocompatibility, and greatly reduces the optothermal damage to the target particles. Interestingly, most biological samples are usually stored in commercial refrigerators with an ambient temperature of about 4 °C.

Furthermore, it is also worth noticing that a series of micro-nanoparticles and biomacromolecules, including PS particles, proteins, and DNAs can turn into negative Soret coefficients under certain temperature conditions [42, 43], which makes this LONT scheme expected to be further applied in more biological experiments. In addition, we also investigated the effect of particle size and type of solution on LONT. The experimental results show that LONT can manipulate nanoparticles (100 nm PS bead) and large particles in micron size (10 μm TiO_2 bead) (see Note S5 in the ESM). According to Eq. S3 in the ESM: $F = 6\pi\eta Ru$, the larger the radius of a particle, the larger the trapping force. Additionally, the Brownian motion of particles with smaller sizes is more intense that it is not conducive to their trapping. Therefore, there exists a limitation for LONT to trap smaller size (< 100 nm) nanoparticles.

We also tested its performance in a commonly used biological buffer of phosphate buffer solution (PBS). Particles are more likely to be trapped and printed on the Au substrate in PBS solution because of the ion effect presented in PBS (discussion can be found in Note S6 in the ESM). Further development mainly focuses on the improvement of existing microfluidic refrigerator device. For example, it can be replaced by a more exquisite and stable temperature control device such as a temperature control console, which can further realize stable and dynamic temperature control of the flow cell. And a microfluidic refrigerator that is compatible with dark-field microscopy is highly preferred, it would enable more clear observation of the manipulation of various kinds of particles. Nevertheless, with its advantages of stable manipulation, good biocompatibility, and trivial optothermal influence, this novel low-temperature optothermal nanotweezers is expected to become a useful tool in the field of biochemistry, synthetic biology, colloidal science, and nanotechnology.

4 Method

Experimental setup

The optical setup of LONT was based on a Nikon Ti2-E inverted microscope. The 785 nm laser used in the experiments was OBIS 785 LX model from Coherent. The objective model was CFI Super Flour 100×, NA = 1.3 (Nikon). The beam splitter (BS) was purchased from Thorlabs (DMSP750B), with a 785 nm laser transmission to reflection ratio of 1:90. The refrigeration plate was made of copper with the customized size that matches the microfluidic chamber. The complementary metal-oxide-semiconductor (CMOS) used in the experiments was a colored camera (Dhyana 400DC, Tucsen) and the CMOS used to measure trapping stiffness was a monochrome camera (DMK 37AUX287). The short-pass filter (< 670 nm, OD = 4.0) was purchased from Edmund.

Acknowledgements

This work was supported by the National Natural Science Foundation of China (Nos. 62275164, 61905145, and 62275168), National Key Research and Development Program of China (No.

2022YFA1200116), Guangdong Natural Science Foundation and Province Project (No. 2021A1515011916), and Shenzhen Science and Technology Planning Project (No. ZDSYS20210623092006020).

Electronic Supplementary Material: Supplementary material (numerical simulation of the temperature; thermophoretic force and thermo-osmotic flow calculation; the trapping stiffness measurement; the trapping of particles of different sizes, including the movie of trapping 10 μm particles (Movie ESM2); and effect of LONT on particle capture in phosphate buffer solution) is available in the online version of this article at https://doi.org/10.1007/s12274-023-5659-1.

References

[1] Ashkin, A.; Dziedzic, J. M.; Yamane, T. Optical trapping and manipulation of single cells using infrared laser beams. *Nature* **1987**, *330*, 769–771.

[2] Grier, D. G. A revolution in optical manipulation. *Nature* **2003**, *424*, 810–816.

[3] Fränzl, M.; Thalheim, T.; Adler, J.; Huster, D.; Posseckardt, J.; Mertig, M.; Cichos, F. Thermophoretic trap for single amyloid fibril and protein aggregation studies. *Nat. Methods* **2019**, *16*, 611–614.

[4] Jiang, H. R.; Wada, H.; Yoshinaga, N.; Sano, M. Manipulation of colloids by a nonequilibrium depletion force in a temperature gradient. *Phys. Rev. Lett.* **2009**, *102*, 208301.

[5] Gargiulo, J.; Brick, T.; Violi, I. L.; Herrera, F. C.; Shibanuma, T.; Albella, P.; Requejo, F. G.; Cortés, E.; Maier, S. A.; Stefani, F. D. Understanding and reducing photothermal forces for the fabrication of Au nanoparticle dimers by optical printing. *Nano Lett.* **2017**, *17*, 5747–5755.

[6] Grigorenko, A. N.; Roberts, N. W.; Dickinson, M. R.; Zhang, Y. Nanometric optical tweezers based on nanostructured substrates. *Nat. Photonics* **2008**, *2*, 365–370.

[7] Babynina, A.; Fedoruk, M.; Kühler, P.; Meledin, A.; Döblinger, M.; Lohmüller, T. Bending gold nanorods with light. *Nano Lett.* **2016**, *16*, 6485–6490.

[8] Blázquez-Castro, A. Optical tweezers: Phototoxicity and thermal stress in cells and biomolecules. *Micromachines* **2019**, *10*, 507.

[9] Volpe, G.; Quidant, R.; Badenes, G.; Petrov, D. Surface plasmon radiation forces. *Phys. Rev. Lett.* **2006**, *96*, 238101.

[10] Min, C. J.; Shen, Z.; Shen, J. F.; Zhang, Y. Q.; Fang, H.; Yuan, G. H.; Du, L. P.; Zhu, S. W.; Lei, T.; Yuan, X. C. Focused plasmonic trapping of metallic particles. *Nat. Commun.* **2013**, *4*, 2891.

[11] Zhang, W. H.; Huang, L. N.; Santschi, C.; Martin, O. J. F. Trapping and sensing 10 nm metal nanoparticles using plasmonic dipole antennas. *Nano Lett.* **2010**, *10*, 1006–1011.

[12] Kang, J. H.; Kim, K.; Ee, H. S.; Lee, Y. H.; Yoon, T. Y.; Seo, M. K.; Park, H. G. Low-power nano-optical vortex trapping via plasmonic diabolo nanoantennas. *Nat. Commun.* **2011**, *2*, 582.

[13] Pang, Y. J.; Gordon, R. Optical trapping of 12 nm dielectric spheres using double-nanoholes in a gold film. *Nano Lett.* **2011**, *11*, 3763–3767.

[14] Braun, M.; Cichos, F. Optically controlled thermophoretic trapping of single nano-objects. *ACS Nano* **2013**, *7*, 11200–11208.

[15] Chen, J. J.; Kang, Z. W.; Kong, S. K.; Ho, H. P. Plasmonic random nanostructures on fiber tip for trapping live cells and colloidal particles. *Opt. Lett.* **2015**, *40*, 3926–3929.

[16] Kang, Z. W.; Chen, J. J.; Wu, S. Y.; Chen, K.; Kong, S. K.; Yong, K. T.; Ho, H. P. Trapping and assembling of particles and live cells on large-scale random gold nano-island substrates. *Sci. Rep.* **2015**, *5*, 9978.

[17] Chen, J. J.; Cong, H. J.; Loo, F. C.; Kang, Z. W.; Tang, M. H.; Zhang, H. X.; Wu, S. Y.; Kong, S. K.; Ho, H. P. Thermal gradient induced tweezers for the manipulation of particles and cells. *Sci. Rep.* **2016**, *6*, 35814.

[18] Lin, L. H.; Hill, E. H.; Peng, X. L.; Zheng, Y. B. Optothermal manipulations of colloidal particles and living cells. *Acc. Chem. Res.* **2018**, *51*, 1465–1474.

[19] Lin, L. H.; Wang, M. S.; Peng, X. L.; Lissek, E. N.; Mao, Z. M.; Scarabelli, L.; Adkins, E.; Coskun, S.; Unalan, H. E.; Korgel, B. A. Opto-thermoelectric nanotweezers. *Nat. Photonics* **2018**, *12*, 195–201.

[20] Chen, J. J.; Loo, J. F. C.; Wang, D. P.; Zhang, Y.; Kong, S. K.; Ho, H. P. Thermal optofluidics: Principles and applications. *Adv. Opt. Mater.* **2020**, *8*, 1900829.

[21] Fränzl, M.; Cichos, F. Hydrodynamic manipulation of nano-objects by optically induced thermo-osmotic flows. *Nat. Commun.* **2022**, *13*, 656.

[22] Wang, X. Y.; Yuan, Y. Q.; Xie, X.; Zhang, Y. Q.; Min, C. J.; Yuan, X. C. Graphene-based opto-thermoelectric tweezers. *Adv. Mater.* **2022**, *34*, 2107691.

[23] Würger, A. Thermal non-equilibrium transport in colloids. *Rep. Prog. Phys.* **2010**, *73*, 126601.

[24] Lin, L. H.; Peng, X. L.; Mao, Z. M.; Wei, X. L.; Xie, C.; Zheng, Y. B. Interfacial-entropy-driven thermophoretic tweezers. *Lab Chip* **2017**, *17*, 3061–3070.

[25] Li, J. G.; Chen, Z. H.; Liu, Y. R.; Kollipara, P. S.; Feng, Y. C.; Zhang, Z. L.; Zheng, Y. B. Opto-refrigerative tweezers. *Sci. Adv.* **2021**, *7*, eabh1101.

[26] Zhou, J. X.; Dai, X. Q.; Jia, B. L.; Qu, J. L.; Ho, H. P.; Gao, B. Z.; Shao, Y. H.; Chen, J. J. Nanorefrigerative tweezers for optofluidic manipulation. *Appl. Phys. Lett.* **2022**, *120*, 163701.

[27] Roder, P. B.; Smith, B. E.; Zhou, X. Z.; Crane, M. J.; Pauzauskie, P. J. Laser refrigeration of hydrothermal nanocrystals in physiological media. *Proc. Natl. Acad. Sci. USA* **2015**, *112*, 15024–15029.

[28] Rahman, A. T. M. A.; Barker, P. F. Laser refrigeration, alignment and rotation of levitated Yb^{3+}: YLF nanocrystals. *Nat. Photonics* **2017**, *11*, 634–638.

[29] Duhr, S.; Braun, D. Why molecules move along a temperature gradient. *Proc. Natl. Acad. Sci. USA* **2006**, *103*, 19678–19682.

[30] Hansen, P. M.; Bhatia, V. K.; Harrit, N.; Oddershede, L. Expanding the optical trapping range of gold nanoparticles. *Nano Lett.* **2005**, *5*, 1937–1942.

[31] De Groot, S. R.; Mazur, P. Non-Equilibrium Thermodynamics. *Am J Phys* **2013**, *31*, 558–559.

[32] Duhr, S.; Braun, D. Thermophoretic depletion follows Boltzmann distribution. *Phys. Rev. Lett.* **2006**, *96*, 168301.

[33] Braibanti, M.; Vigolo, D.; Piazza, R. Does thermophoretic mobility depend on particle size. *Phys. Rev. Lett.* **2008**, *100*, 108303.

[34] Russel, W. B.; Saville, D. A.; Schowalter, W. R. *Colloidal Dispersions*; Cambridge University Press: Cambridge, 1991.

[35] Anderson, J. L. Colloid transport by interfacial forces. *Annu. Rev. Fluid Mech.* **1989**, *21*, 61–99.

[36] Bregulla, A. P.; Würger, A.; Günther, K.; Mertig, M.; Cichos, F. Thermo-osmotic flow in thin films. *Phys. Rev. Lett.* **2016**, *116*, 188303.

[37] Donner, J. S.; Baffou, G.; McCloskey, D.; Quidant, R. Plasmon-assisted optofluidics. *ACS Nano* **2011**, *5*, 5457–5462.

[38] Wong, W. P.; Halvorsen, K. The effect of integration time on fluctuation measurements: Calibrating an optical trap in the presence of motion blur. *Opt. Express* **2006**, *14*, 12517–12531.

[39] Ding, H. R.; Kollipara, P. S.; Lin, L. H.; Zheng, Y. B. Atomistic modeling and rational design of optothermal tweezers for targeted applications. *Nano Res.* **2021**, *14*, 295–303.

[40] Haidacher, D.; Vailaya, A.; Horváth, C. Temperature effects in hydrophobic interaction chromatography. *Proc. Natl. Acad. Sci. USA* **1996**, *93*, 2290–2295.

[41] Southall, N. T.; Dill, K. A.; Haymet, A. D. J. A view of the hydrophobic effect. *J. Phys. Chem. B* **2002**, *106*, 521–533.

[42] Iacopini, S.; Piazza, R. Thermophoresis in protein solutions. *Eur. Lett.* **2003**, *63*, 247–253.

[43] Iacopini, S.; Rusconi, R.; Piazza, R. The "macromolecular tourist": Universal temperature dependence of thermal diffusion in aqueous colloidal suspensions. *Eur. Phys. J. E* **2006**, *19*, 59–67.